

BOLD and Sodium MRI of the Human Kidney: Preliminary Experience with Patients

Y. Rosen^{1,2}, G. Bodonyi-Kovacs^{2,3}, N. Hindman^{1,2}, N. M. Rofsky^{1,2}, R. E. Lenkinski^{1,2}, and F. H. Epstein^{2,3}

¹Radiology, Beth Israel Deaconess Medical Center, Boston, MA, United States, ²Harvard Medical School, Boston, MA, United States, ³Nephrology Division, Beth Israel Deaconess Medical Center, Boston, MA, United States

Introduction

Traditionally imaging studies in acute or chronic renal failure are performed only to exclude morphological findings such as obstruction (secondary to stones, hemorrhage or tumor) or renal artery stenosis, while functional studies rely mainly on laboratory tests of the plasma or urine. MRI provides an opportunity to non-invasively study parameters of renal function and physiology as well as pathophysiological changes, and their spatial distribution in the kidneys. Specifically, we have studied renal oxygenation using Blood Oxygenation Level-Dependent (BOLD) MRI, and the spatial distribution of sodium concentration using ²³Na MRI. BOLD MRI has been used to study renal oxygenation patterns in humans, and proved to adequately describe the physiological relative medullary hypoxia, and the changes induced by diuretic agents (1). ²³Na MRI of the kidneys has been able to characterize the specific modulations in pathologies as hydronephrosis and acute tubular necrosis in the intact rat kidney (2,3). ²³Na MRI of the human kidneys, as was recently developed in our lab, enabled the determination of the corticomedullary sodium gradient, and has been proven sensitive to changes in water homeostasis in the body (4). Both imaging techniques are able to map these physiological parameters in the various regions of the kidneys at 2-3 mm in-plane spatial resolution, and therefore may lead to new insights regarding the pathogenic processes underlying various renal diseases. This ongoing initial study is aimed at monitoring the modulations in renal oxygenation levels and in the corticomedullary sodium gradient along the progression of various types of renal failure, investigating the possible correlation between these two parameters, and determining whether the pathophysiological patterns observed are diffuse or focal in presentation.

Methods

Subjects: MR studies were performed on 5 patients and 1 healthy volunteer so far. Three of the patients had transplanted kidneys, two of them with chronic renal failure (CRF) and 1 with normal renal function, and the other 2 patients had CRF of their intact kidneys.

Data acquisition: MRI scans were performed on a 3.0 T scanner (Signa LX, General Electric, Waukesha, WI). The subjects lay supine and entered the magnet with their feet first. The imaging protocol included two parts:

Part I – Anatomical imaging and BOLD, using a torso array 8-channel coil:

- 1) Fast 3D SPGR (LAVA) with TR/TE=4/1.8 ms, flip angle=10°, FOV=40 cm, slice thickness=5 mm, matrix=256x192, 0.8 phase FOV sampled.
- 2) FGRE in/out of phase, 2D, TR=250 ms, flip angle=70°, FOV=40 cm, slice thickness=5 mm, slice spacing=0, matrix=320x160, 0.9 phase FOV sampled.
- 3) BOLD imaging using a 3D multiple GRE sequence, with an echo train of 8 echoes, TE's ranging from 2 to 23 ms, TR=25.3, flip angle=10°, BW=83.3 KHz, FOV=40x40x50 cm, slice thickness=5 mm (10 slices prescribed, 6 are eventually reconstructed), matrix=256x160, 0.7x0.7 phase FOV sampled, acq. time=23 sec.

The sequence was supplied by GE, in collaboration with Pottumarthy V. Prasad, PhD, Northwestern University, Chicago, Illinois.

Part II – Reference proton images (body coil) followed by ²³Na imaging of the kidney using a sodium surface coil:

- 1) FGRE in/out of phase, 2D, TR=250 ms, flip angle=70°, FOV=40 cm, slice thickness=15 mm, slice spacing=0, matrix=320x160, 0.8 phase FOV sampled.
- 2) ²³Na MRI using a 3D-GRE sequence modified for multinuclear imaging, with FOV=38x38x24 cm, matrix size=128x128x16, TE/TR =1.8/30 ms, 24 averages, acquisition time=24 min. The short TE was achieved by applying a 66% partial Fourier echo, along with a hard, non-slice selective, 300 μsec RF excitation pulse.

All scans were prescribed to acquire coronal images of intact kidneys or sagittal images of transplanted kidneys. In each part the scans were prescribed with matched slice locations. All scans except for the ²³Na MRI were acquired during breathholds.

Data processing: The anatomical images were evaluated for kidneys size, morphological findings and corticomedullary differentiation. The BOLD data was processed off-line using the freeware ImageJ (5) to fit each pixel intensity curve to an exponential signal decay. The resulting T₂* maps were converted to pixel-by-pixel R₂* maps (R₂*=1/T₂*). The quality of fit (r²) maps, showed r²>0.98 for all renal pixels. The sodium time domain data was filtered with a 2D Fermi filter and reconstructed to complete the non-symmetric k-space data prior to the FFT.

Results

The normally functioning kidneys showed preserved corticomedullary differentiation in all regions of the kidneys in the anatomical images, as shown in Fig.1a. In the correlating R₂* maps, the physiological relative hypoxia in the medullary tissue was clearly evident (Fig.1b). Mean medullary R₂* was 33 Hz, and mean cortical R₂* was 16 Hz, values in agreement with previous reports (6). In the CRF kidneys, the R₂* maps mostly showed no clear corticomedullary differentiation, as shown in Fig 1c. Generally the cortex was less oxygenated while the physiological medullary hypoxia was lost.

²³Na images of a healthy kidney normally show high signal in the renal medullary regions (Fig. 2a), representing the physiologically high sodium concentration in the medulla necessary for normal urine

concentration function. A comparison between a surface function of the signal intensity (Fig. 2b) and a scheme of the human kidney (Fig. 2c) revealed a clear corticomedullary sodium gradient in accordance with the multi-papilla structure of the human kidney. A similar pattern was also demonstrated in the normally functioning transplanted kidney. In the CRF kidneys, this distinct pattern of corticomedullary sodium gradients was not evident in many areas of the renal parenchyma. Interestingly, regions in the kidneys that demonstrated a preserved corticomedullary sodium gradient, correlated well with the presence of medullary hypoxia in the same regions (Fig. 3).

Conclusions

MRI of the kidneys can serve as a non-invasive tool to map both the renal oxygenation level and the sodium concentration function in a quantitative manner. Our preliminary results suggest that CRF may involve regional loss of corticomedullary differentiation, associated with the loss of both the ability to concentrate sodium and with reduced hypoxia in these regions. The differences in renal function and oxygenation between regions of the diseased kidneys suggest that the nature of functional loss may be focal and not globally diffuse as commonly assumed, and that more accurate histological diagnosis might be made if image-guided biopsies were performed.

The surprisingly increased oxygenation in the medulla of CRF kidneys may reflect lower oxygen demand due to reduced functionality, and may also serve to explain the decrease in erythropoietin production in some CRF patients. Further quantitative analyses of the R₂* distribution and the sodium gradients are still ongoing, as well as further optimization of the ²³Na imaging acquisition and processing protocol. Additional scans to evaluate renal perfusion (for example using arterial spin labeling) may complete the information renal MRI can provide regarding the balance between oxygen supply (perfusion), oxygen demand (mostly determined by the sodium concentration function), and actual oxygenation level in various types of renal diseases. Potential clinical applications may include: assessment of the severity of renal dysfunction (especially in patients with unreliable laboratory tests, as in hepato-renal syndrome), monitoring disease progression and therapy effects, and targeting image-guided biopsies.

References: 1) Li et al. J Magn Reson Imaging. 2004 Nov; 20(5):901-4. 2) Maril et al., Kidney Int. 2004 Mar; 65(3): 927-35. 3) Maril et al. Kidney Int. 2006 Feb;69(4):765-8. 4) Maril et al. Magn Reson Med. 2006 Nov 6; [Epub] 5) <http://rsb.info.nih.gov/ij/> 6) Tumkur et al. Invest Radiol. 2006 Feb;41(2):181-4.

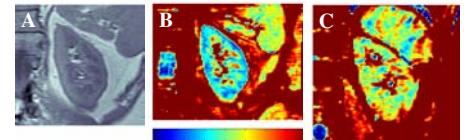


Figure 1. A) An Anatomical proton image of a healthy kidney. B) R₂* map of a healthy kidney. C) R₂* map of a kidney with CRF.

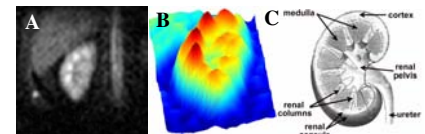


Figure 2. A) A sodium image of a healthy kidney. B) A surface plot of the signal intensity of A. C) A scheme of the human kidney.

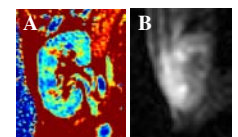


Figure 3. A) R₂* map of a transplanted kidney with CRF. B) A sodium image of the same kidney.